Behaviors of tribrachial edge flames and their interactions in a triple-port burner

Kazuhiro YAMAMOTO, Yusuke ISOBE, Naoki HAYASHI, Hiroshi YAMASHITA
Department of Mechanical Science and Engineering, Nagoya University
Furo-cho, Chikusa-ku, Nagoya, Aichi 464-8603, Japan

Suk Ho CHUNG
Clean Combustion Research Center
King Abdullah University of Science and Technology
Thuwal 23955-6900, Kingdom of Saudi Arabia

Abstract
In a triple-port burner, various non-premixed flames have been observed previously. Especially for the case with two lifted flames, such configuration could be suitable in studying interaction between two tribrachial flames. In the present study, the flame characteristics have been investigated numerically by adopting a reduced kinetic mechanism in the triple-port burner. Four different types of flame configurations, including two attached flames, inner lifted/outer attached flames, inner attached/outer lifted flames, and twin lifted flames, were successfully simulated depending on the flow conditions. The representative edge propagation speed of a single lifted flame or an upstream lifted flame in the case of twin lifted flames increased as the liftoff height became higher. In the twin lifted flames, the inner lifted flame was affected appreciably when the other flame was located further upstream such that the lifted flame located further downstream encountered the axial velocity acceleration induced by the gas expansion from the lifted flame located upstream, while thermal effects were not observed since the temperature of the incoming flow toward the lifted flame was not affected. A unique flip-flop behavior between the inner and outer flames, observed experimentally previously, was successfully captured in the simulation such that the inner lifted flame became attached to the nozzle as the liftoff height of the outer lifted flame grew higher with an increase in the outer air velocity.

Keywords
Non-premixed flame; Lifted flame; Liftoff height; Tribrachial edge flame; Numerical simulation

1. Introduction

Non-premixed flames in a mixing layer play interesting roles under various combustion conditions. An example is a lifted flame in a jet in which the fuel and the oxidizer are partially premixed. The flame edge typically has a tribrachial (or triple) flame structure, consisting of a lean and a rich premixed flame wings and a trailing diffusion flame [1-6]. This type of lifted flame is stabilized by the balance between the propagation speed of the edge flame and the local axial flow velocity. Many fundamental studies have been conducted to investigate the liftoff height behavior [7-12].

Particle image velocimetry (PIV) techniques have revealed that the velocity along the streamline direction in a tribrachial edge flame gradually decreases toward the leading-edge of the lifted flame to a minimum value [13-15], which is reasonably close to the laminar burning velocity [1,3,8,16,17]. The streamline divergence toward the convex premixed flame wings reduces the local velocity in front of a tribrachial flame. As a result, the propagation speed of the edge flame can be larger than a laminar burning velocity, resembling the Landau's hydrodynamic instability phenomenon [6,11,12,14].

Typically, isolated lifted flames either in a uniform flow of a two-dimensional rectangular system or an axisymmetric configuration have been considered [1-6,11]. Recently, direct numerical simulations (DNS) of turbulent lifted flames [18-20] have demonstrated that the incoming flow balances with the local burning velocity of the lifted flame.

In advanced direct-injection spark ignition (DISI) engines operated under stoichiometric conditions, mixtures are typically stratified. In such a situation, the flame propagation after ignition may be controlled by tribrachial edge flames. Because a large number of flamelets could exist under such turbulent conditions, the interaction between flames (flamelets) and flow is expected to be very complex [20-25]. Therefore, a relatively simple flow configuration is desirable to investigate the interaction among tribrachial flames with flow fields. Examples are two lifted edge flames in a slot burner with multiple inlets of fuel and air [26] or a triple port burner [27].

A triple port burner has three concentric tubes. Air flows through both the central and outermost tubes and fuel flows through the annulus between the two air tubes. Since there are central and outer airflows next to the fuel flow, two (an inner and an outer) flames are formed [27]. Compared with a typical co-axial burner, the contact area between the fuel and air in a triple port burner is larger because of the introduction of the central air jet, which promotes mixing of the fuel and air and subsequently reactions [28]. Depending on the flow conditions, four different flame configurations have been observed previously in a triple port burner. These include attached flames, inner lifted/outer attached flames, inner attached/outer lifted flames, and twin lifted flames. One of the interesting finding was a flip-flop behavior between the inner and outer flames, which is shown in **Fig. 1**. These photos of flames were recorded at 15 fps by changing U_{3A} from 1.0 to 1.1 m/s at U_{1A} = 0.6 m/s and U_{2F} = 0.6 m/s, where U_{1A}, U_{2F}, and U_{3A} are the average velocities of central air, fuel, and outer air, respectively. The result indicates that the inner lifted flame becomes re-attached, while the outer flame is lifted with the small change in the outer air velocity. The objective of the present study is to numerically simulate such behaviors observed previously in the triple port burner [27].

Fig.1

2. Numerical analysis

Figure 2 shows the computational domain and coordinate system. The numerical model, including the scheme and boundary conditions, was discussed in detail previously [27]. Time-dependent conservation equations of momentum, energy, and species were solved by the SIMPLE method [10] on an axisymmetric configuration with methane fuel. A finite difference procedure with staggered grids was adopted. The third-order upwind difference scheme was used for convective term. The time advance was made by using Euler's fully implicit method [4, 29-31]. The computational domain was 16.8 mm in the radial direction and −1 to 200 mm in the axial direction. Similar to the experimental conditions [27], the radii of the central air nozzle, the fuel nozzle and the outer air nozzle were 5, 7 and 13.5 mm, respectively. The thickness of each nozzle was 1 mm. The grid size was 0.1 mm, and a grid

dependence was confirmed in preliminary tests. When the grid was coarse, the grid size dependence was observed. They were converged when the grid size was smaller than 0.1 mm. At the nozzle exits, parabolic velocity profiles were assigned. The temperature of the fuel and air was 297 K. A methane-air skeletal kinetic mechanism was used for the consideration of computational time, consisting of 16 chemical species and 25 elementary reactions, which has been proposed during the workshop on "Reduced Kinetic Mechanisms and Asymptotic Approximations for Methane-Air Flames" held at the University of California at San Diego in 1989 [32]. The calculated stoichiometric laminar burning velocity was 0.43 m/s, which is in reasonable agreement with various experimental data reported. This skeletal mechanism has also been successfully used previously for relatively large scale non-premixed methane jet flames [33] and highly turbulent premixed flames [34].

In the simulation, the average fuel velocity, U_{2F}, was fixed at 0.6 m/s, and the central air velocity, U_{1A}, was 0.4 m/s (case A) or 0.7 m/s (case B), while the outer air velocity, U_{3A}, was varied. The air outside the outermost tube was ambient air with a uniform velocity (0.01 m/s). At the outlet and the side boundaries, the convective boundary condition was set, where the gradient of a scalar such as temperature was zero.

Fig.2

3. Results and discussion

3.1. Flame transition in case A

First, the flame transition from nozzle-attached to outer lifted flame (case A) is discussed. Distributions of the heat release rate at U_{3A} = 0.2, 0.5, and 0.8 m/s are shown in Fig. 3. To show the flame structure clearly, these images are enlarged in the radial direction. As the outer air velocity (U_{3A}) increases, a transition from two attached flames to inner attached/outer lifted flames is observed. Details of the tribrachial flame structure are described below.

The liftoff height (L_f) and the maximum heat release rate (Q_{max}) of the outer flame are shown in Fig. 4. The heat release rate is at its maximum at the leading edge of the lifted flame because of the premixed flame

wings of the tribrachial edge flame and the stoichiometry of the tribrachial point. Here, the liftoff height is defined based on the axial position of the maximum heat release rate. First, we compared the predicted liftoff height with experimental results. Since the liftoff height in experiments was slightly slanted and fluctuated, the time and space averaged value was used. For example, for the case of U_{1A} = 0.4 m/s and U_{3A} = 0.4 m/s, L_f of the outer flame was 3.2 mm, which was close to the value of the simulation of 3.9 mm.

As seen in Fig. 4, both L_f and Q_{max} increase as U_{3A} increases. For U_{3A} = 0.2 m/s, the outer flame is attached with $L_f \sim 1$ mm corresponding to a quenching distance. As the outer lifted flame stabilizes further downstream, the leading-edge flame intensifies. The edge behavior of a tribrachial flame is strongly influenced by the fuel concentration gradient, which is related with the scalar dissipation rate. This point has been extensively discussed for a single lifted flame in a free jet, where it has demonstrated that the upstream fuel concentration gradient was linearly proportional to the curvature of tribrachial edge flame [35]. Consequently, the fuel concentration gradient affects the curvature of the premixed wing of the tribrachial edge [36-38], and thus the flow redirection effect [3]. As the liftoff height increases with U_{3A}, the concentration gradient in front of the edge decreases such that the tribrachial edge flame strengthens with a higher heat release rate, since scalar dissipation rate decreases.

Fig.3

Fig.4

To further illustrate this, the axial velocity along the axial direction v_z at the radial position of the maximum heat release rate, which corresponds to the leading edge of the lifted flame shown in **Fig. 5** with U_{3A} varying from 0.2 to 0.8 m/s. Except for the attached flame case of U_{3A} = 0.2 m/s, the axial velocity gradually decreases toward the downstream as the jet spreads, reaches its minimum, and then increases sharply as the gas expands. It is confirmed that the cold gas upstream of the lifted flame is not preheated such that thermal effects are not observed because of the nature of premixed flame having typical preheat zone thickness of O(1 mm). The local dip in the axial velocity is due to the streamline divergence ahead of the lifted flame edge [14,15,19]. Here, the local minimum velocity in **Fig. 5** can be defined as a representative edge propagation speed of the

leading edge lifted flame (S_e). It is expected that the inflow velocity balances with the propagation speed of leading edge of the stationary lifted flame. **Figure 6** shows the edge propagation speed, S_e, plotted in relation to the liftoff height. Note that S_e and the laminar burning velocity can differ because of the slantedness of a flame edge at the tribrachial point, as discussed in detail previously [39]. The result shows that S_e of the outer lifted flame increases with U_{3A}, exhibiting a reasonable correlation with the heat release rate shown in **Fig. 4**. An increase in the edge propagation speed at a higher liftoff height has been reported in the case of the single lifted flame in a uniform flow [2,3], which was explained by effects of flame curvature and the scalar dissipation rate [1,3,5].

Fig.5

Fig.6

3.2. Flame transition in case B

In case B, a somewhat different flame behavior is observed when U_{3A} increases at fixed U_{1A} (= 0.7 m/s). As U_{3A} increases, both the inner and outer stationary flames are lifted. The results of the liftoff heights with U_{3A} are shown in **Fig. 7**. At U_{3A} = 0 m/s, both flames are attached. At U_{3A} = 0.2 m/s, the inner attached flame has a transition to a lifted flame, while the outer flame remains attached. The inner flame stabilizes further downstream when U_{3A} increases. Around U_{3A} = 0.4 m/s, the outer flame also has a transition to a lifted flame. Consequently, twin lifted flames are stabilized. Up to $U_{3A} \leq 1.0$ m/s, the liftoff height of the inner flame is always larger than that of the outer flame. When U_{3A} is slightly larger than 1.0 m/s, the liftoff heights of both flames become comparable. As U_{3A} increases further, the inner flame has a second transition to become a nozzle-attached flame. This sudden change in the liftoff heights (the flip-flop behavior captured in **Fig. 1)** can also be observed in the simulation. Again, we compared liftoff heights in case B with experimental results. For example, for U_{3A} = 0.5 m/s, L_f of the outer flame was 5 mm and that of the inner flame was 33 mm. On the other hand, for U_{3A} = 1.0 m/s, L_f of the outer flame was 38 mm and that of the inner flame was 42 mm. Since these values were close to those of simulation results in Fig. 7, we could confirm the validation of the numerical

simulation. In the following, this transition behavior will be further discussed.

Fig.7

3.2.1. Transition to inner lifted/outer attached flames

When U_{3A} is increased, the inner flame lifts first. The position of the inner leading-edge flame is examined in **Fig. 8.** The radial and axial positions are plotted for every 0.1 m/s change in U_{3A}. As the inner flame is lifted, its flame edge position initially migrates toward the axis. This is because the stoichiometric contour, where the edge flame is formed, is located on the air side given the stoichiometric fuel-to-oxidizer mass ratio. The flame edge movement is appreciable when U_{3A} changes from 0.2 to 0.3 m/s, corresponding to the liftoff of the inner flame. In accordance with $U_{1A} > U_{3A}$, the axial velocity is larger around the center axis, inducing the flow toward the center axis. Once the inner flame edge moves inward, it advances into the region with large axial velocity, and, consequently, the liftoff height increases. In case A, on the other hand, the internal air flow velocity of 0.4 m/s is slightly smaller than the predicted laminar burning velocity of a stoichiometric methane-air mixture of 0.43 m/s as mentioned previously. In that case, even if the external air flow velocity increases, the inner flame is not lifted.

Fig.8

3.2.2. Transition to twin lifted flames

When U_{3A} is greater than 0.4 m/s, the outer flame is also lifted. The value of U_{3A} at which this transition is observed reasonably corresponds to the laminar burning velocity of the stoichiometric methane-air mixture. In other words, for $U_{3A} > 0.4$ m/s, the incoming flow does not balance with the burning velocity, so that the outer flame is lifted to form twin lifted flames. As shown in **Fig. 7**, when U_{3A} further increases, the liftoff height increases.

The axial velocity profile is examined to evaluate the edge propagation speed of the inner and outer lifted flames. The results are shown in **Fig. 9**. These distributions are obtained at the radial position of the maximum heat release rate, corresponding to the leading edge of the inner or outer flame is formed. Similar to case A in

Fig. 5, the axial velocity becomes minimum near the edge position of lifted flame. The axial velocity of the outer flame in **Fig. 9a** decreases monotonically toward to the leading edge of the flame, and it increases sharply across the flame by expansion of the gas. For the inner flame in **Fig. 9b**, the axial velocity of the incoming flow first decreases along the axial direction, then increases toward the leading edge of the flame. This can be attributed to the fact that there is an outer flame located more upstream, which could affect the flow ahead of the inner flame. Again, a velocity dip and a sharp velocity increase crossing the flame can be observed.

To elucidate further, the heat release rate and axial velocity profiles at $U_{3A} = 0.8$ m/s are shown in **Fig. 10**, in which the region close to the leading edges of both lifted flames is the focus. The tribrachial structure of the edge flame can be clearly identified, with a lean premixed flame (LPF) wing, a rich premixed flame (RPF) wing, and a trailing diffusion flame (DF), all extending from the tribrachial point (TP). The slope of the flame wing at TP is slanted toward the fuel region, which has been previously observed experimentally due to the velocity gradient in the upstream region and the stoichiometric oxidizer to fuel mass ratio [37].

Fig.9

Fig.10

The outer flame is located further upstream as compared with the inner flame. There exists an inward radial velocity component toward the inner flame (circled region in **Fig. 9b**). This is the reason why the axial velocity profiles of the inner flames in **Fig. 9b** are somewhat different from those of the outer flame shown in **Figs. 5** and **9a**. Due to this diverging flow across the outer premixed flame wing, the upstream of the inner flame region accelerates, leading to an increase in the liftoff height of the inner flame.

The representative edge propagation speed of the lifted flame corresponding to the local minimum velocity in **Fig. 9** is shown in **Fig. 11**, where the velocity of the inner or outer flame is characterized by the liftoff height. In the outer flame, as the liftoff height becomes higher, the edge propagation speed increases, resembling single lifted flame cases with uniform flow [3,5]. Because the outer flame is located further upstream, the influence of the inner flame is expected to be weak on the behavior of outer flame edge. In this regard, the minimum velocity range is close to that of case A, except that the liftoff height of case B is much higher with increased U_{3A}.

While the edge propagation speed of the inner flame shows a somewhat different behavior. The velocity is near constant for $U_{3A} < 0.8$ m/s, and it decreases at higher liftoff height. As seen in **Fig. 7**, the distance between the inner and outer flames becomes smaller at increased U_{3A}. The variation in the minimum velocity for the inner flame could be caused by the interaction between the inner and outer flames. Also note that, when U_{3A} is 1.0 m/s, the minimum velocity of the inner flame is reduced to a smaller value than that of the outer flame.

Fig.11

3.2.3. Transient behavior from twin lifted flames to inner attached/outer lifted flames

Thus far, stationary flames have been discussed. Considering the importance of unsteady tribrachial flames that could occur in direct-injection spark ignition engines during flame propagation, we also studied the unsteady behavior of a flame when U_{3A} increases from 1.0 m/s to 1.1 m/s. In this case, as seen in **Fig. 7**, the liftoff heights of the inner and outer flames are reversed, resulting in the outer flame edge located further upstream. Since the inward flow component is generated by gas expansion near the edge of the outer lifted flame toward the inner flame, the outer flame pushes the inner flame away from the nozzle. Once the liftoff height of the inner flame is comparable to that of the outer flame, this effect is mitigated.

Here, the edge propagation speed of the inner flame is estimated from the flame displacement speed relative to the local minimum flow velocity [6]. The resulting edge speed is plotted with the liftoff height in **Fig. 12**. As compared with **Fig. 11**, as the inner flame approaches the nozzle (decreasing liftoff height), the edge propagation speed becomes slower. This is consistent with the characteristics of the edge propagation speed observed previously in that the speed decreases with the upstream fuel concentration gradient [36,40]. Note that as the inner edge flame approaches the nozzle, the concentration gradient is decreased in the fuel/air mixing layer.

Figure 13 shows the transient behavior of liftoff heights of these flames, where the time $t = 0$ corresponds to the time when U_{3A} changes from 1.0 to 1.1 m/s. For $t < 100$ ms, the liftoff height of the outer

flame gradually increases, whereas that of the inner flame remains nearly unchanged. When the liftoff height of the outer flame becomes higher than that of the inner flame at around t = 130 ms, the inner flame edge starts to migrate slowly toward the nozzle. After t = 200 ms, the displacement speed of the inner flame edge accelerates and subsequently the edge flame reattaches to the nozzle rather rapidly.

The decrease in the edge speed with decreasing liftoff height alone cannot explain the reattachment behavior of the inner lifted flame. For this, we examine the flow field. **Figure 14** shows the profiles of the heat release rate distributions with velocity vectors at t = 40, 120, and 240 ms. The rim between the internal air and fuel nozzles is located at 5 mm < r < 6 mm, and that between the fuel and the external air nozzles is located at 7 mm < r < 8 mm. Consequently, the flow speed is quite slow in the wake regions above these rims [39]. As shown in **Fig. 10**, when the liftoff height of the inner flame is higher than that of the outer flame, the inner flame is pushed toward the center axis by the flow induced by the outer flame, and it is thus located in the higher axial velocity region. However, once both liftoff heights are comparable, the above-mentioned effect is mitigated, and the inner flame moves outward and then enters the wake region having a low axial velocity. As a consequence, after t = 120 ms, the inner lifted flame starts to migrate toward the nozzle. Therefore, even though the edge speed is decreasing, the inner flame propagates upstream along the region with low axial flow velocity. This indicates that the balance between the incoming flow and the edge speed remains important for such propagating flame. Such behavior could be important in determining transient behaviors in turbulent flames with stratified concentration field, where the structure and flow near tribrachial edge flames with be fluctuating rapidly [42]. Thus, the above interaction between the inner and outer lifted tribachial flames could provide useful insight in modeling turbulent combustion with multiple flamelets.

Fig.12
Fig.13
Fig.14

4. Conclusions

The flame behavior and the flow field in the triple port burner were numerically examined. The

following conclusions were drawn.

(1) Depending on the flow conditions, the inner flame and/or the outer flame is lifted. In the velocity profile of a single lifted flame or the lifted flame located upstream in the case of twin lifted flames, the axial velocity gradually decreases, approaches to its minimum, and then increases very rapidly, which is similar to the behavior of a single lifted flame in uniform flow field. The local minimum velocity was represented as edge propagation speed of the lifted flame. In the lifted flame located downstream, the axial velocity of the incoming flow first decreases and then increases toward the leading edge of the lifted flame. The temperature of the incoming flow toward the lifted flame is not influenced such that thermal effects were not observed.

(2) The flame transition depends on U_{1A}. In case A (U_{1A} = 0.4 m/s), only the outer flame is lifted as U_{3A} increases. When the liftoff height is higher, the heat release rate of the lifted flame increases and the local minimum velocity is higher. The lifted flame stabilizes at the position where the edge propagation speed of the lifted flame and the incoming flow velocity are balanced.

(3) In case B (U_{1A} = 0.7 m/s), as U_{3A} increases, both the inner and outer flames are lifted. The lifted flame located downstream faces the flow induced by the lifted flame located upstream. As a result, the liftoff height of the inner flame increases until U_{3A} is 1.0 m/s even though the internal air flow velocity remains constant. Once the liftoff heights of the inner and outer flames are comparable, the effect of the outer flame on the flow field near inner flame is mitigated and the inner flame attaches to the nozzle.

(4) Based on the transient behavior of twin lifted flames changing to inner attached/outer lifted flames, we calculated the edge propagation speed of the inner flame from the flame displacement speed relative to the local minimum flow velocity. As the inner flame approaches the nozzle with a lower liftoff height, the edge propagation speed decreases. The inner flame propagates upstream along the low incoming flow, and as a result, a unique flip-flop behavior between the inner and outer flames can be observed. Similar to a stationary flame, the balance between the edge propagation speed and the inflow velocity is important to transient flame behaviors.

Acknowledgments

The authors thank Prof. Amable Liñán of Universidad Politecnica de Madrid in Spain for very helpful discussions on lifted flames in the triple port burner.

References

[1] J.W. Dold, *Combust. Flame* 76 (1989) 71-88.

[2] P.N. Kioni, B. Rogg, K.N.C. Bray, A. Liñán, *Combust. Flame* 95 (1993) 276–290.

[3] G.R. Ruetsch, L. Vervisch, A. Liñán, *Phys. .Fluids* 7 (1995) 1447-1454.

[4] H. Yamashita, M. Shimada, and T. Takeno, *Proc. Combust. Inst.* 26 (1996) 1226-1233.

[5] J. Boulanger, and L. Vervisch, *Combust. Flame* 130 (2002) 1–14.

[6] E. Fernandez-Tarrazo, M. Vera, A. Linan, *Combust. Flame* 144 (2006) 261–276.

[7] F. Takahashi, W. J. Schmoll, *Proc. Combust. Inst.* 23 (1990) 677-683.

[8] S.H. Chung, B.J. Lee, *Combust. Flame* 86 (1991) 62–72.

[9] M.S. Cha, S.H. Chung, *Proc. Combust. Inst.* 26 (1996) 121-128.

[10] T. Fujimori, D. Riechelmann, J. Sato, *Proc. Combust. Inst.* 27 (1998) 1149-1155.

[11] S. Ghosal, L. Vervisch, *Combust. Flame* 123 (2001) 646–655.

[12] M. Hirota, T. Yokomori, et al., *Proc. Combust. Inst.* 31 (2007) 893-899.

[13] L. Muñiz, M.G. Mungal, *Combust. Flame* 111 (1997) 16-31.

[14] T. Plessing, P. Terhoeven, N. Peters, M.S. Mansour, *Combust. Flame* 115 (1998) 335–353.

[15] A. Upatnieks, J.F. Driscoll, C.C. Rasmussen, S.L. Ceccio, *Combust. Flame* 138 (2004) 259–272.

[16] H.G. Im, J.H. Chen, *Combust. Flame* 119 (1999) 436–454.

[17] I.K. Puri, S.K. Aggarwal, S. Ratti, R. Azzoni, *Combust. Flame* 124 (2001) 311–325.

[18] Y. Mizobuchi, S. Tachibana, J. Shinio, S. Ogawa, T. Takeno, *Proc. Combust. Inst.* 29 (2002) 2009-2015.

[19] Y. Mizobuchi, J. Shinio, S. Ogawa, T. Takeno, *Proc. Combust. Inst.* 30 (2005) 611-619.

[20] C.S. Yoo, E.S. Richardson, R. Sankaran, J.H. Chen, *Proc. Combust. Inst.* 33 (2011) 1619-1627.

[21] K.A. Watson, K.M. Lyons, J.M. Donbar, C.D. Carter, *Combust. Flame* 117 (1999) 257–271.

[22] A. Joedicke, N. Peters, M. Mansour, *Proc. Combust. Inst.* 30 (2005) 901-909.

[23] S. Noda, H. Mori, Y. Hongo, M. Nishioka, *JSME Int. J.* 48 (2005) 75-82.

[24] S. Ishizuka, T. Motodamari, D. Shimokuri, *Proc. Combust. Inst.* 31 (2007) 1085-1092.

[25] H. Wang, M. Juddoo, S.H. Starner, A.R. Masri, S.B. Pope, *Proc. Combust. Inst.* 34 (2013) 1251-1259.

[26] S. Kostka, W.F. Carnell Jr., M.W. Renfro, *Combust. Flame* 154 (2008) 82-95.

[27] K. Yamamoto, S. Kato, Y. Isobe, N. Hayashi, H. Yamashita, *Proc. Combust. Inst.* 33 (2011) 1195-1201.

[28] K. Yamamoto, M. Takemoto, *Fuel Processing Technol*. 107 (2013) 99-106.

[29] H. Yamashita, G., Kushida, and Takeno, T., *Proc. R. Soc. London, Ser. A*, 431 (1990) 301-314.

[30] H. Yamashita, G. Kushida, and T. Takeno, *Proc. Combust. Inst.* 24 (1992) 311-316.

[31] D. Zhao, H. Yamashita, K. Kitagawa, N. Arai, T. Furuhata, *Combust. Flame* 130 (2002) 352-360.

[32] M.D. Smooke, *Reduced Kinetic Mechanisms and Asymptotic Approximations for Methane-Air Flames*, Springer-Verlag, Berlin, Germany, 1991.

[33] S. James, F. Jaberi, *Combust. Flame* 123 (2000) 465-487.

[34] G. Fru, D. Thévenin, G. Janiga, *Energies* 4 (2011) 878-893.

[35] J. Lee, S.H. Chung, *Combust. Flame* 127 (2001) 2194–2204.

[36] Y.S. Ko, S.H. Chung, *Combust. Flame* 118 (1999) 151–163.

[37] S.K. Aggarwal, Prog. Energy *Combust. Sci.* 35 (2009) 528–570.

[38] F. Bisetti, S.M. Sarathy, M. Toma, S.H. Chung, *Proc. Combust. Inst.* 35 (2014) in press.

[39] M.K. Kim, S.H. Won, S.H. Chung, *Proc. Combust. Inst.* 31 (2007) 901-908.

[40] J. Lee, S.H. Won, S.H. Jin, S.H. Chung, O. Fujita, K. Ito, *Combust. Flame* 134 (1999) 411–420.

[41] I. Sakurai, et al., *Proc. Combust. Inst.* 34 (2013) 2727-2734.

[42] A.M. Steinberg, R. Sadanandan, C. Dem, P. Kutne, W. Meier, *Proc. Combust. Inst.* 34 (2013) 1499-1507.

Figure captions

Fig. 1 Photos of the flip-flop behavior between inner and outer flames by changing U_{3A} from 1.0 to 1.1 m/s at $U_{1A} = 0.6$ m/s, $U_{2F} = 0.6$ m/s, recorded at 15 fps.

Fig. 2 Computational domain and coordinate system.

Fig. 3 Distributions of the heat release rate in case A for $U_{3A} = 0.2$ (a), 0.5 (b), and 0.8 m/s (c).

Fig. 4 Liftoff height and heat release rate of the outer flame in case A.

Fig. 5 Distributions of the axial velocity of the outer flame in case A.

Fig. 6 Liftoff height and burning velocity of the outer flame in case A.

Fig. 7 Variations in the liftoff height by changing U_{3A} in case B.

Fig. 8 Position of the inner leading-edge lifted flame in case B.

Fig. 9 Distributions of the axial velocity in case B; (a) outer flame, (b) inner flame.

Fig. 10 Distributions of the (a) heat release rate and (b) axial velocity at $U_{3A} = 0.8$ m/s in case B.

Fig. 11 Liftoff height and edge propagation speed in case B; (a) outer flame, (b) inner flame.

Fig. 12 Liftoff height and edge propagation speed of the inner flame in case B.

Fig. 13 Time variations in the liftoff height of the inner and outer flames by changing U_{3A} from 1.0 to 1.1 m/s is shown. The flow conditions are $U_{1A} = 0.7$ m/s, $U_{2F} = 0.6$ m/s.

Fig. 14 Distributions of the heat release rate with a velocity vector in case B are shown, by changing U_{3A} from 1.0 to 1.1 m/s at (a) $t = 40$ ms, (b) 120 ms, (c) 240 ms.

(a) (b) (c) (d)

Fig. 1 Photos of the flip-flop behavior between inner and outer flames by changing U_{3A} from 1.0 to 1.1 m/s at U_{1A} = 0.6 m/s, U_{2F} = 0.6 m/s, recorded at 15 fps.

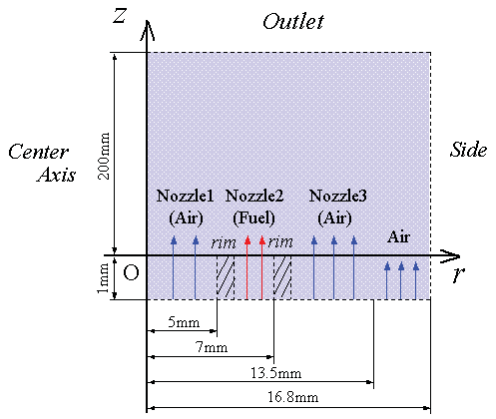

Fig. 2 Computational domain and coordinate system.

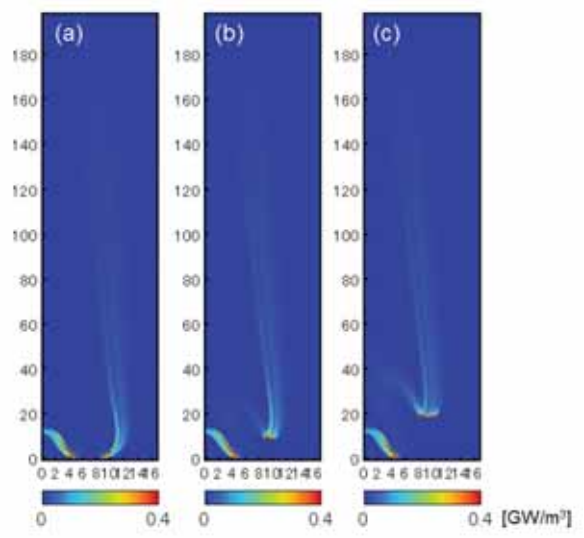

Fig. 3 Distributions of the heat release rate in case A for $U_{3A} = 0.2$ (a), 0.5 (b), and 0.8 m/s (c).

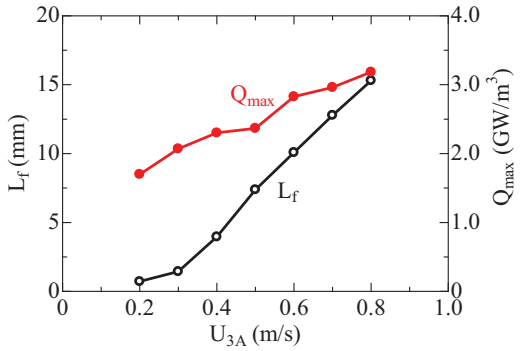

Fig. 4 Liftoff height and heat release rate of the outer flame in case A.

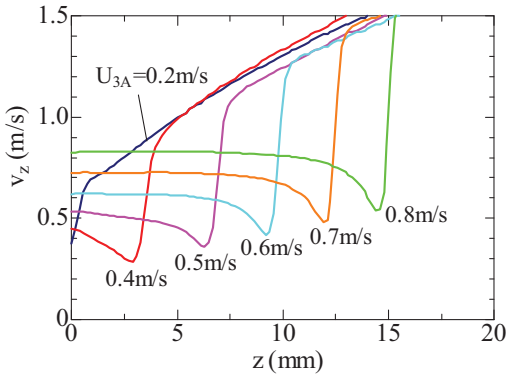

Fig. 5 Distributions of the axial velocity of the outer flame in case A.

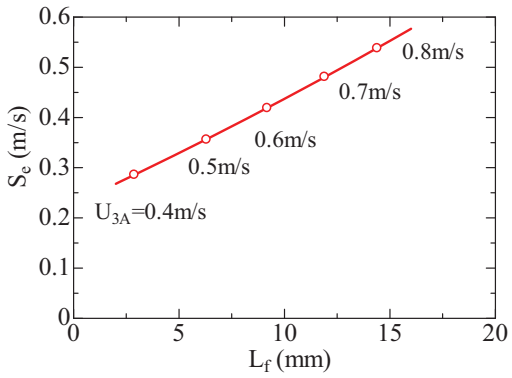

Fig. 6 Liftoff height and burning velocity of the outer flame in case A.

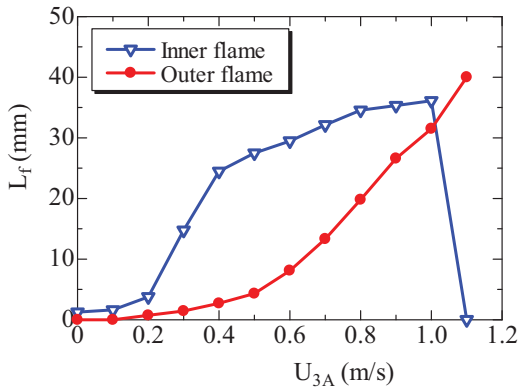

Fig. 7 Variations in the liftoff height by changing U_{3A} in case B.

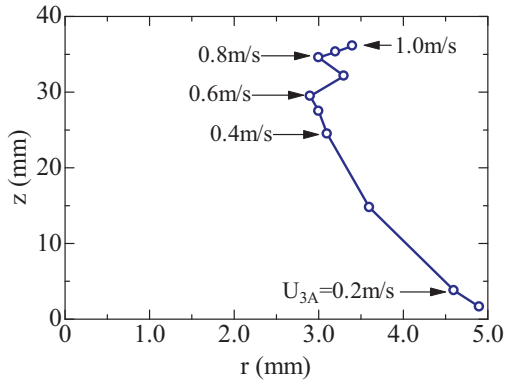

Fig. 8 Position of the inner leading-edge lifted flame in case B.

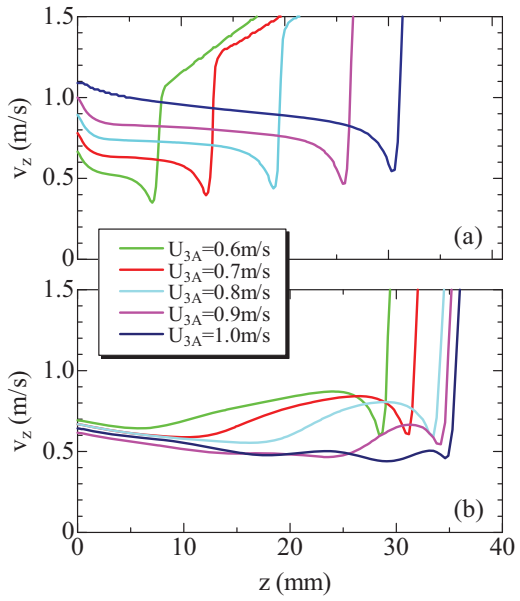

Fig. 9 Distributions of the axial velocity in case B; (a) outer flame, (b) inner flame.

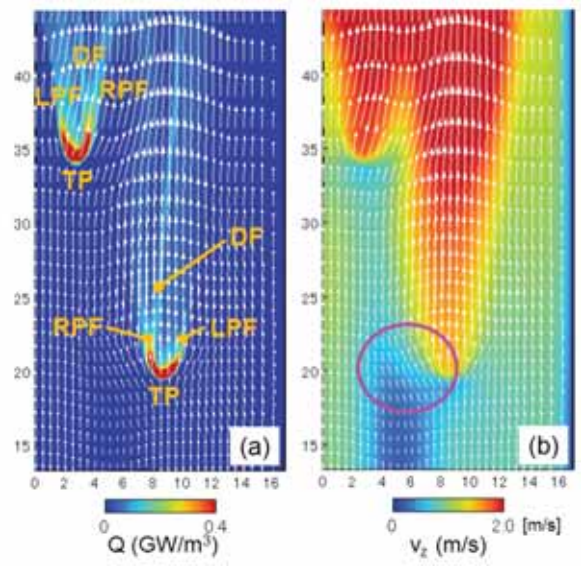

Fig. 10 Distributions of (a) heat release rate and (b) axial velocity at $U_{3A} = 0.8$ m/s in case B.

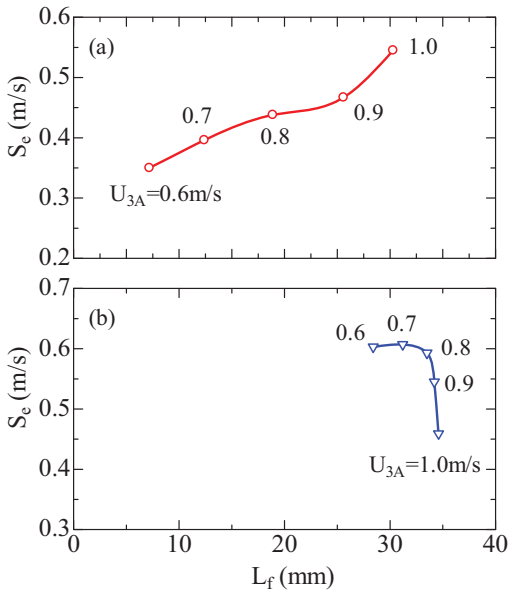

Fig. 11 Liftoff height and edge propagation speed in case B; (a) outer flame, (b) inner flame.

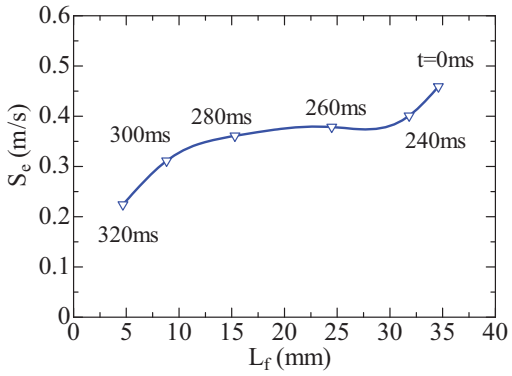

Fig. 12 Liftoff height and edge propagation speed of the inner flame in case B.

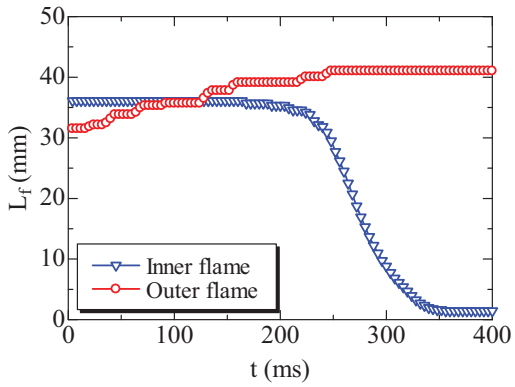

Fig. 13 Time variations in the liftoff height of the inner and outer flames by changing U_{3A} from 1.0 to 1.1 m/s is shown. The flow conditions are $U_{1A} = 0.7$ m/s, $U_{2F} = 0.6$ m/s.

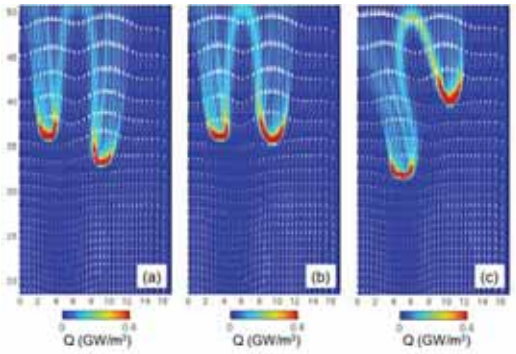

Fig. 14 Distributions of the heat release rate with a velocity vector in case B are shown, by changing U_{3A} from 1.0 to 1.1 m/s at (a) t = 40 ms, (b) 120 ms, (c) 240 ms.

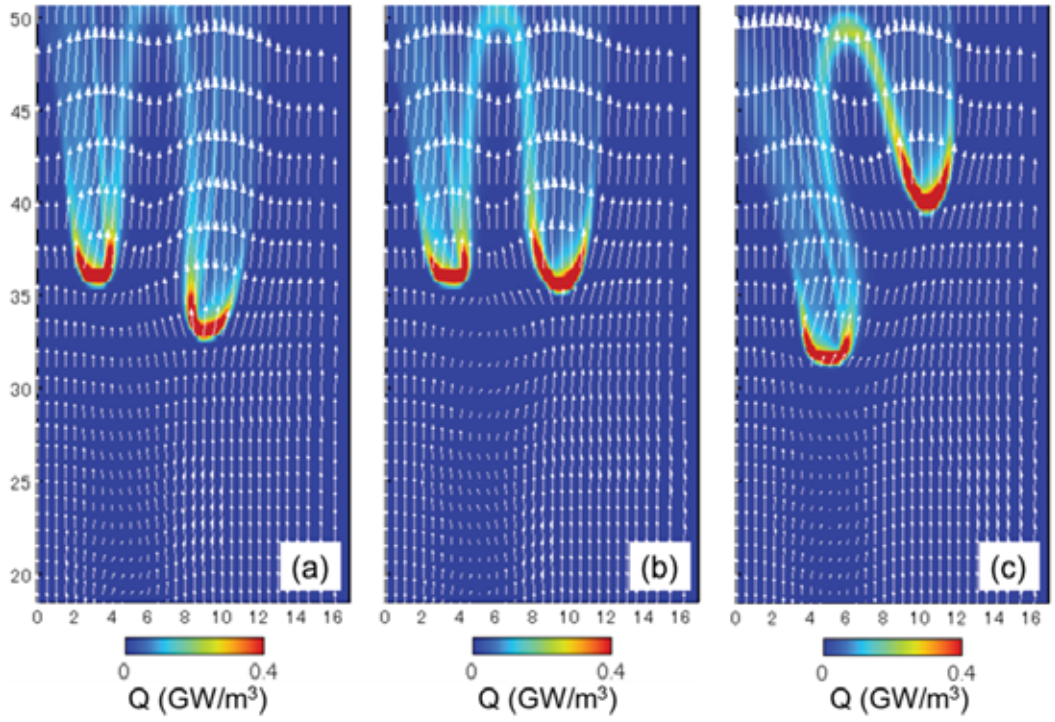

Fig. 14 (enlarged)